

Tuning Genetic Clocks Employing DNA Binding Sites

Shridhar Jayanthi^{1,2} and Domitilla Del Vecchio^{2*}

1 Electrical Engineering and Computer Science, University of Michigan, Ann Arbor, MI, USA

2 Mechanical Engineering, Massachusetts Institute of Technology, Cambridge, MA, USA

*** E-mail: ddv@mit.edu**

Abstract

Periodic oscillations play a key role in cell physiology from the cell cycle to circadian clocks. The interplay of positive and negative feedback loops among genes and proteins is ubiquitous in these networks. Often, delays in a negative feedback loop and/or degradation rates are a crucial mechanism to obtain sustained oscillations. How does nature control delays and kinetic rates in feedback networks? Known mechanisms include proper selection of the number of steps composing a feedback loop and alteration of protease activity, respectively. Here, we show that a remarkably simple means to control both delays and effective kinetic rates is the employment of DNA binding sites. We illustrate this design principle on a widely studied activator-repressor clock motif, which is ubiquitous in natural systems. By suitably employing DNA target sites for the activator and/or the repressor, one can switch the clock “on” and “off” and precisely tune its period to a desired value. Our study reveals a design principle to engineer dynamic behavior in biomolecular networks, which may be largely exploited by natural systems and employed for the rational design of synthetic circuits.

Introduction

Periodic oscillations are essential for biological phenomena such as cell cycle regulation and circadian rhythms [1, 2]. Several studies attribute these oscillations to bio-molecular clocks composed of genes arranged in feedback networks [3, 4]. Of the several arrangements that may produce oscillations, *activator-repressor* motifs are recurrent in several natural systems [3, 5]. These motifs comprise an activator module that is self activated and that activates a repressor module. The repressor module, in turn, represses the activator (Figure 1a). This motif has been shown to be remarkably robust to biological noise [5], leading

to synthetic implementations as model systems to study natural clocks [6–9].

Independently of the specific topology of the network, the presence of delays in feedback loops has long been recognized as a key mechanism to obtain periodic behavior and to tune the clock period (see the review by [1] and the study by [10]). Similarly, a key (related) parameter controlling periodic behavior is the relative value among protein decay rates [11, 12]. For the activator-repressor motif, for example, analytical studies have demonstrated that a crucial mechanism for sustained oscillations is the time-scale difference between the activator and the repressor dynamics, that is, the repressor dynamics should be sufficiently slower than the activator dynamics [13, 14]. This is, to some extent, qualitatively similar to having a delay in the negative feedback from the repressor to the activator. How does nature realize and tune delays and kinetic rates in feedback motifs? Known ways to increase a delay in a feedback or to make the feedback slower include either decreasing the decay rates of species involved in the negative feedback and/or increasing the number of steps in the feedback loop (see, for example, [10, 14, 15]).

Recent studies of modularity in biomolecular circuits have revealed that excess of DNA targets to a protein can slow down the protein’s dynamics [16, 17]. This effect, called *retroactivity*, is a consequence of changes in the dynamics of the system due to the sequestration of the protein from the network of interactions composing the system. Basically, the protein is “busy” in binding the targets and hence takes longer to perform its function in the system to which it belongs. In the context of modularly designing circuits in synthetic biology, this is an undesired effect (similar to impedance in electrical circuits) that occurs when two modules are interconnected by a transcription factor of one module binding to DNA target sites in the other module. From the perspective of a natural system, however, this loading effect may provide a simple method to tune delays and change the effective kinetic rates without changing the “hardware” of the network.

In this work, we demonstrate that indeed DNA target sites can be employed as a powerful design parameter to finely tune and control the dynamic behavior of a biomolecular circuit, the activator-repressor clock of Figure 1a in particular. Specifically, we illustrate how one can change the dynamics of an activator-repressor clock utilizing DNA binding sites (*load*) with affinity to each of the species. Initially, a mechanism to switch an oscillator “on” or “off” is shown depending on which node (the activator or repressor) the load is being added to. Robustness of this behavior to intrinsic noise is verified by employing stochastic simulation of a mechanistic model of the clock. Finally, a method to tune the period of the clock by employing a carefully chosen amount of load to both nodes is demonstrated.

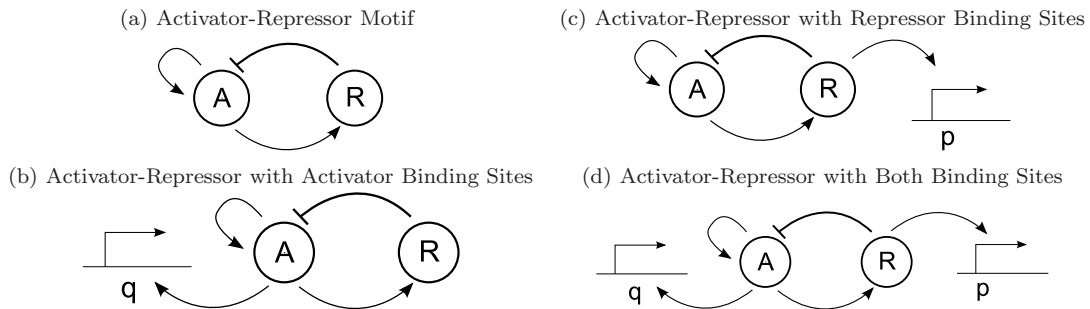


Figure 1. *Illustration of the systems analyzed in this paper.* Diagram (a) illustrates the activator-repressor motif. Diagram (b) and (c) illustrate the systems after the addition of DNA binding sites with affinity to the activator and the repressor, respectively. Diagram (d) illustrates the case in which both types of DNA binding sites are present.

Results

We consider a general model for a two-component clock incorporating both positive and negative feedback loops based on the activator-repressor configuration of [6] and illustrated in Figure 1a. Oscillations for activator-repressor clocks often arise from Hopf bifurcation, wherein a stable equilibrium point bifurcates into an unstable equilibrium and a stable periodic orbit when a key parameter is changed [9, 13, 14, 18, 19]. In the models surveyed in the literature, the fundamental mechanism responsible for this oscillatory behavior is well captured by a reduced two-dimensional model that describes the rate of change of the activator and repressor concentrations. This model is obtained by taking into account that the period of oscillations occurs in a timescale slower than the dynamics of multimerization, binding and dissociation interactions, so that quasi-steady state approximations can be made [6, 9, 19]. Additionally, it has been shown that transcription and translation can be lumped into a one-step expression model with no impact to the dynamics of interest [5, 14]. Following these prior works, we also focus on a reduced two-dimensional model.

In the system of Figure 1a, activator protein A promotes its own expression as well as the expression of repressor protein R. Protein R, in turn, represses expression of protein A. Let K_{m1} be the apparent dissociation constant between the activator protein and its DNA binding site and K_{m2} be the apparent dissociation constant between repressor protein and its DNA binding site [20] (see SI for details). For any species X, we denote in italics X its concentration. Consider the concentration of A and R given in units of their respective dissociation constants $a := A/K_{m1}$ and $r := R/K_{m2}$. Considering a one-step

model for protein expression, the dynamics for this system can be represented by

$$\begin{aligned}\dot{a} &= -\delta_A a + f_1(a, r) \\ \dot{r} &= -\delta_R r + f_2(a),\end{aligned}\tag{1}$$

in which δ_A and δ_R model protein decay (due to either dilution or degradation) and functions f_1 and f_2 model expression rates and take the form of the standard Hill functions [2]

$$f_1(a, r) = \frac{\beta_1 a^m + \beta_2}{1 + a^m + r^n} \text{ and } f_2(a) = \frac{\beta_3 a^m + \beta_4}{1 + a^m},\tag{2}$$

in which β_1 and β_3 are the maximal expression rates, β_2 and β_4 represent the basal expression, and m and n are the Hill coefficients of the affinity between the proteins A and R and their respective binding sites. The mathematical derivation of this reduced nondimensional model is given in the SI. In the sequel, we refer to system (1) as the *isolated system*.

We assume that the values of the parameters are such that system (1) has a unique equilibrium point. We give conditions for which this assumption holds when either $m = 1$ or $m = 2$ in the SI. In particular, it is shown that when $m = 1$, the system always presents a unique and stable equilibrium and, therefore, no oscillatory behavior can be observed. When $m = 2$ the uniqueness of the equilibrium is guaranteed under the following conditions: (i) the value of β_2 must be sufficiently smaller than the maximal expression rate of the activator, which is proportional to β_1 ; (ii) β_2 must be non-zero; (iii) the maximal expression rate of the repressor must be larger than the maximal expression rate of the activator; (iv) the smaller β_2 becomes, the smaller β_4 must be. In the general case ($m > 2$), results related to existence and uniqueness of equilibria require a case by case analysis, which is out of the scope of this work. The results from this paper, do not explicitly impose conditions on the Hill coefficients m and n and only assume the uniqueness of the equilibrium (a^*, r^*) for system (1).

Since system (1) is a two-dimensional system, Poincaré-Bendixson theorem [21] can be employed to obtain conditions for the existence of a periodic orbit. Specifically, one must show that the trajectories of the system are bounded in a compact set and that the equilibrium point is unstable and not locally a saddle.

The following proposition shows that the trajectories of system (1) are bounded in a compact set.

Proposition 1. *There exists a constant $D \in \mathbb{R}_+$ such that the set $K = \{(a, r) \in \mathbb{R}_+^2 \mid a^2 + r^2 \leq D^2\}$ is a*

positively invariant set under the vector field defined by system (1) and its equilibrium $(a^*, r^*) \in K$.

Proof. Note that $f_1(a, r)$ and $f_2(a)$ are positive bounded functions in the domain \mathbb{R}_+^2 . Let $M_1 = \sup_{(a,r) \in \mathbb{R}_+^2} \{f_1(a, r)\}$ and $M_2 = \sup_{a \in \mathbb{R}_+} \{f_2(a)\}$. First, notice that for $a = 0, \dot{a} > 0$ according to (1). Similarly, for $r = 0, \dot{r} > 0$. The quadrant \mathbb{R}_+^2 is, therefore, a positively invariant set. Define $\delta^* := \min\{\delta_A, \delta_R\}$ and $M := \max\{M_1, M_2\}$. Consider the positive definite function $v(a, r) = a^2/2 + r^2/2$. Using the chain rule, we obtain

$$\begin{aligned} \frac{dv(a, r)}{dt} &= -\delta_A a^2 - \delta_R r^2 + a f_1(a, r) + r f_2(a) \\ &\leq -\delta^* a^2 - \delta r^2 + aM + rM \\ &= -\delta^* \left(a - \frac{M}{2\delta^*}\right)^2 - \delta^* \left(r - \frac{M}{2\delta^*}\right)^2 + \frac{M^2}{2(\delta^*)^2}. \end{aligned}$$

From the above, it is clear that $\dot{v}(a, r) < 0$ on the exterior of a circle with center $(M/2\delta^*, M/2\delta^*)$ and radius $\sqrt{2}M/2\delta^*$. Therefore, for any $D > \max\{\sqrt{2}M/2\delta^*, a^*, r^*\}$, $\dot{v}(a, r) < 0$ along the arc defined by the boundary of K . Hence, K is a positively invariant set that contains the equilibrium (a^*, r^*) . \square

To show that the equilibrium point is unstable and not locally a saddle, consider the Jacobian matrix of system (1) calculated at the equilibrium:

$$J_0 = \begin{bmatrix} -\delta_A + \frac{\partial f_1(a^*, r^*)}{\partial a} & \frac{\partial f_1(a^*, r^*)}{\partial r} \\ \frac{\partial f_2(a^*)}{\partial a} & -\delta_R \end{bmatrix}, \quad (3)$$

and denote by $\text{tr}(J_0)$ and $\det(J_0)$ the trace and the determinant of J_0 , respectively. The eigenvalues of the Jacobian are given by

$$\lambda_{1,2} = \frac{\text{tr}(J_0) \pm \sqrt{\text{tr}(J_0)^2 - 4 \det(J_0)}}{2},$$

hence the equilibrium point is unstable and not locally a saddle if $\text{tr}(J_0) > 0$ and $\det(J_0) > 0$. Given the specific expression of the Jacobian in (3), the equilibrium (a^*, r^*) of system (1) is unstable and not locally a saddle if the following conditions are fulfilled:

- (i) $\delta_R \left(\delta_A - \frac{\partial f_1(a^*, r^*)}{\partial a} \right) - \frac{\partial f_1(a^*, r^*)}{\partial r} \frac{\partial f_2(a^*)}{\partial a} > 0$ ($\det(J_0) > 0$);
- (ii) $\frac{\partial f_1(a^*, r^*)}{\partial a} - \delta_A - \delta_R > 0$ ($\text{tr}(J_0) > 0$).

System (1) satisfying conditions (i) and (ii) presents periodic orbits and will be referred to as *Functional Clock*.

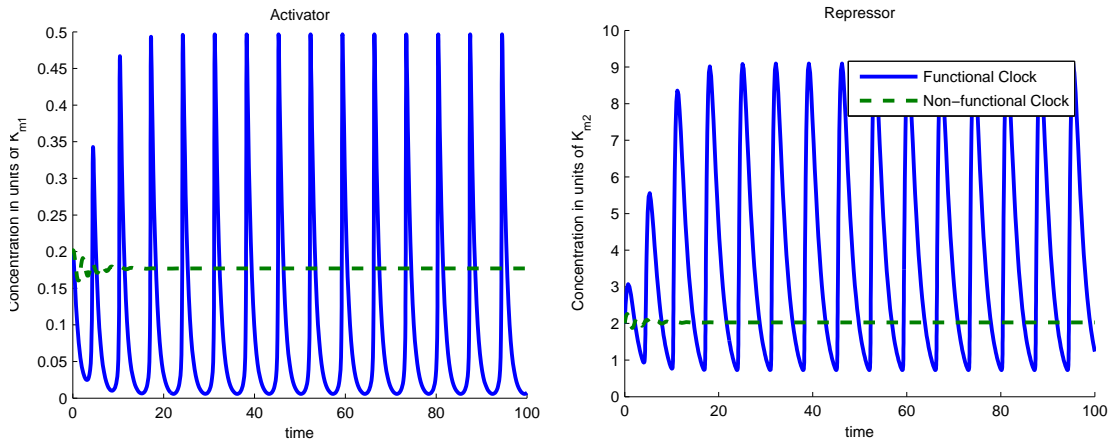


Figure 2. Effect of the trace of the Jacobian on the stability of the equilibrium. The above plots illustrate the trajectories of system (1) for both Functional and Non-Functional Clocks. The parameters in the simulation were $\beta_1 = \beta_3 = 100$, $\beta_2 = .04$, $\beta_4 = .004$ and $\delta_A = 1$. In the Functional Clock, $\delta_R = 0.5$ whereas in the Non-Functional Clock, $\delta_R = 1.5$. Parameters β_1 and β_3 were chosen to give about 500-2000 copies of protein per cell for activated promoters. Parameters β_2 and β_4 were chosen to give about 1-10 copies per cell for non-activated promoters.

Condition (ii) highlights a crucial design principle for the activator-repressor clock. In fact, assume that $\frac{\partial f_1(a^*, r^*)}{\partial a} - \delta_A > 0$, which is satisfied if the self activation is sufficiently strong. Then, condition (ii) can be satisfied if $\frac{\partial f_1(a^*, r^*)}{\partial a} - \delta_A$ is sufficiently larger than δ_R . This, in turn, implies that the timescale of the activator dynamics are sufficiently faster than that of the repressor dynamics. Hence, a central mechanism for the appearance of a limit cycle is a fast activator dynamics compared to the repressor dynamics. Retroactivity on a species due to downstream binding sites has been shown to slow down the species dynamics [16, 17]. It follows that downstream binding sites can be employed to vary the relative speeds between the activator and the repressor dynamics. Hence, we will also consider the non-oscillating version of system (1) that does not satisfy condition (ii), referred to as *Non-Functional Clock*. The non-functional clock is given by system (1) in which, in addition to condition (i), the following condition is satisfied:

$$(ii)', \quad 0 < \frac{\partial f_1(a^*, r^*)}{\partial a} - \delta_A < \delta_R.$$

Figure 2 illustrates how conditions (ii) and (ii)' generate a Functional and a Non-Functional Clock, respectively, by changing the value of parameter δ_R .

In this work, we study how the addition of binding sites to the repressor or activator can switch system (1) between the Functional Clock and the Non-Functional Clock behavior, with no change to the parameters of the original system (1).

Switching the clock off by loading the activator

In this section, we show the effect of additional DNA binding sites for the activator in a Functional Clock. Specifically, consider system (1) satisfying conditions (i) and (ii). The addition of DNA binding sites q_A with affinity to the activator A, which binds as homomers, illustrated in Figure 1b, is modeled by the following chemical reaction



in which D_1 represents the complex formed by A and q . We will assume that the affinity between these promoter sites and the activator protein A is given by the apparent dissociation constant $K_{m1} = \sqrt[m]{k_{b1}/k_{a1}}$, identical to the affinity of A to the promoters in the isolated clock. Additionally, we assume the total concentration of binding sites $\bar{q}_A = (q_A + D_1)/K_{m1}$ to be constant. Let the complex concentration D_1 be given in units of K_{m1} using the nondimensional variable $d_1 = D_1/K_{m1}$. The dynamics of the system after nondimensionalization are given by

$$\begin{aligned} \dot{a} &= -\delta_A a + f_1(a, r) + mG_1\delta_A d_1 - mG_1\delta_A a^m(\bar{q}_A - d_1) \\ \dot{r} &= -\delta_R r + f_2(a) \\ \dot{d}_1 &= -G_1\delta_A d_1 + G_1\delta_A a^m(\bar{q}_A - d_1), \end{aligned} \quad (5)$$

in which $G_1 = k_{b1}/\delta_A$ models the timescale separation between the dissociation rate and the protein degradation. A mathematical derivation for this model is found in the SI. Since binding and unbinding reactions can occur in the order of milliseconds, they are in a timescale significantly faster than expression and degradation of proteins, which occur in the order of minutes [2]. As a result, parameter G_1 is very large. This fact allows to employ a singular perturbation argument [22, 23] to facilitate the analysis of

this system. To this end, define the small parameter $\epsilon := 1/G_1$ and re-write system (5) as

$$\begin{aligned}\dot{a} &= -\delta_A a + f_1(a, r) + \frac{m}{\epsilon} (\delta_A d_1 - \delta_A a^m (\bar{q}_A - d_1)) \\ \dot{r} &= -\delta_R r + f_2(a) \\ \dot{d}_1 &= \frac{1}{\epsilon} (-\delta_A d_1 + \delta_A a^m (\bar{q}_A - d_1)).\end{aligned}\tag{6}$$

In order to reduce this system to standard singular perturbation form, we perform the change of variables $y = md_1 + a$, so that system (6) becomes

$$\dot{y} = -\delta_A (y - md_1) + f_1(y - md_1, r)\tag{7}$$

$$\dot{r} = -\delta_R r + f_2(y - md_1)\tag{8}$$

$$\epsilon \dot{d}_1 = -\delta_A d_1 + \delta_A (y - md_1)^m (\bar{q}_A - d_1),\tag{9}$$

which is in standard singular perturbation form. Setting $\epsilon = 0$ one obtains from (9) the solution $d_1 = \frac{\bar{q}_A a^m}{a^m + 1} := \phi_1(a)$. This equation defines the slow manifold, which can be shown to be locally exponentially stable (see SI). Hence, system (7) is well approximated by the reduced system obtained by replacing d_1 by its expression on the slow manifold $\phi_1(a)$. Specifically, we have that

$$-\delta_A a + f_1(a, r) = \dot{y} = m \dot{d}_1 + \dot{a} = m \frac{d\phi_1(a)}{da} \dot{a} + \dot{a},$$

from which we obtain that

$$\dot{a} = \frac{1}{1 + m \frac{d\phi_1(a)}{da}} (-\delta_A a + f_1(a, r)).$$

Denoting

$$\mathcal{S}_A(a, \bar{q}_A) := \frac{1}{1 + \frac{d\phi_1(a)}{da}} = \frac{1}{1 + m \bar{q}_A a^{m-1} (1 + a^m)^{-2}},$$

the reduced system in the original coordinates is given by

$$\begin{aligned}\dot{a} &= \mathcal{S}_A(a, \bar{q}_A) (-\delta_A a + f_1(a, r)) \\ \dot{r} &= -\delta_R r + f_2(a).\end{aligned}\tag{10}$$

Since $\mathcal{S}_A(a, \bar{q}_A) \neq 0$, the equilibria of (10) are the same as the ones of (1). Therefore, if (1) has a unique equilibrium (a^*, r^*) , this will also be a unique equilibrium of (10). Also, we have that $0 < \mathcal{S}_A(a, \bar{q}_A) \leq 1$ and that $\mathcal{S}_A(a, \bar{q}_A)$ is a strictly monotonically decreasing function of the amounts of DNA binding sites \bar{q}_A . Hence, in system (10), the dynamics of the activator have been slowed down compared to the original isolated system (1). That is, the *effective* kinetic rate of the activator dynamics is now decreased by a factor equal to $\mathcal{S}_A(a, \bar{q}_A)$. Note additionally that

$$\lim_{\bar{q}_A \rightarrow \infty} \mathcal{S}_A(a, \bar{q}_A) = 0 \text{ and } \mathcal{S}_A(a, 0) = 1. \quad (11)$$

The Jacobian of system (10) calculated at the equilibrium is given by

$$J_A(\bar{q}_A) = \begin{bmatrix} \mathcal{S}_A^*(\bar{q}_A) \left(-\delta_A + \frac{\partial f_1(a^*, r^*)}{\partial a} \right) & \mathcal{S}_A^*(\bar{q}_A) \frac{\partial f_1(a^*, r^*)}{\partial r} \\ \frac{\partial f_2(a^*)}{\partial a} & -\delta_R \end{bmatrix}, \quad (12)$$

in which we use the shorthand notation $\mathcal{S}_A^*(\bar{q}_A) := \mathcal{S}_A(\bar{q}_A, a^*)$. We have $\det(J_A(\bar{q}_A)) = \mathcal{S}_A^*(\bar{q}_A) \det(J_0) > 0$ from condition (i) and that

$$\text{tr}(J_A(\bar{q}_A)) = \mathcal{S}_A^*(\bar{q}_A) \left(-\delta_A + \frac{\partial f_1(a^*, r^*)}{\partial a} \right) - \delta_R.$$

Hence, while the addition of load does not change the sign of the determinant of the Jacobian, it can change the sign of the trace. For large enough load, because of (11), the trace becomes negative and the equilibrium point becomes stable. Hence, the periodic orbit disappears (see the SI for details). Figure 3 a shows the effect of load on system (5).

For the value of \bar{q}_A for which $\text{tr}(J_A(\bar{q}_A)) = 0$, the eigenvalues of the Jacobian are imaginary, hence the system goes through a Hopf bifurcation. A continuation study shows that the Hopf bifurcation is present also in the full three-state system (5). In particular, the amounts of load needed to switch the clock off is about four times the amplitude of the activator oscillations. For the specific choice of parameters in this example, the amount of load required to stop this clock is of the same order of the dissociation constant K_{m1} , which usually amounts to a low concentration. For example, for the NRI activator used in the oscillator in [6], $K_{m1} \approx 10pM$ [24] which amounts to approximately 10 copies of the binding site per cell in *E. coli*.

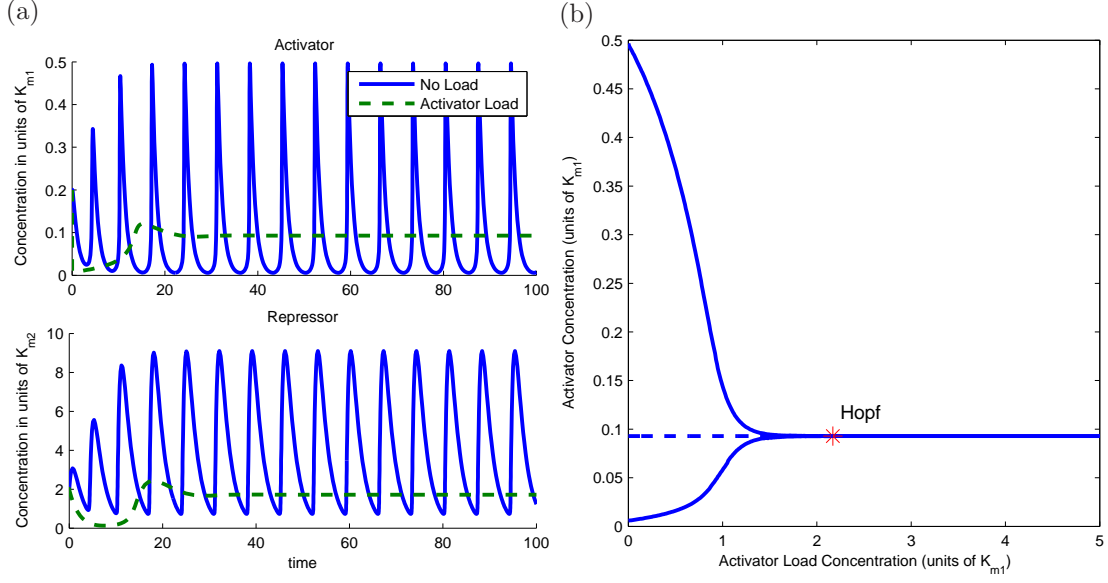


Figure 3. (a) *Load to the Activator can stop a Functional Clock.* The plots illustrate the trajectories of system (5) with two different amounts of load. The parameters in the simulation were $\beta_1 = \beta_3 = 100$, $\beta_2 = .04$, $\beta_4 = .004$, $\delta_A = 1$, $\delta_R = 0.5$, $G_1 = 100$, $m = 2$ and $n = 4$. The amount of DNA binding sites in the system with no load is $\bar{q}_A = 0$ whereas in the system with activator load is $\bar{q}_A = 20$. (b) *Bifurcation diagram with load as parameter.* A continuation of the equilibrium as a function of the load parameter \bar{q}_A shows that, for this set of parameters, the amount of load to the activator required to stop the clock is on the order of the affinity coefficient K_{m1} , with the bifurcation occurring at $\bar{q}_A = 2.17$. The analysis was made on the full system (5) with the same parameters as before. The solid lines indicate a stable trajectory (the limit cycle to the left side of the Hopf bifurcation point and the equilibrium point to the right side of the Hopf bifurcation point). The dotted line indicates an unstable equilibrium point.

Switching the clock on by loading the repressor

We now consider a Non-Functional Clock and show how it can be turned into a Functional Clock by adding load to the repressor. Specifically, consider system (1) satisfying conditions (i) and (ii)'. We model here the addition of DNA binding sites q_R with affinity to the repressor R, similar to the binding sites found in the original clock. This interaction, illustrated in Figure 1c, is modeled by the following chemical reaction



in which D_2 represents the complex formed by the R and q_R . Let the affinity between the repressor and the binding sites is given by the apparent dissociation constant $K_{m2} = \sqrt{k_{b2}/k_{a2}}$. Let $d_2 := D_2/K_{m2}$ be the nondimensional concentration of complexes and $\bar{q}_R = (q_R + D_2)/K_{m2}$ be the total nondimensional

concentration of binding sites. The nondimensionalized dynamics of the system are given by

$$\begin{aligned}\dot{a} &= -\delta_A a + f_1(a, r) \\ \dot{r} &= -\delta_R r + f_2(a) + n\delta_R G_2 d_2 - n\delta_R G_2 r^n (\bar{q}_R - d_2) \\ \dot{d}_2 &= -\delta_R G_2 d_2 + \delta_R G_2 r^n (\bar{q}_R - d_2),\end{aligned}\tag{14}$$

in which $G_2 := k_{b2}/\delta_R$ models timescale separation between the dissociation rate of the complex D_2 and the repressor decay rate. It is possible to reduce the order of system (14) by a similar technique employed in the previous section. To this end, define $\epsilon := G_2^{-1}$. Define also the variable $y := r + nd_2$, system (14) can be taken to the standard singular perturbation form

$$\begin{aligned}\dot{a} &= -\delta_A a + f_1(a, y - nd_2) \\ \dot{y} &= -\delta_R (y - nd_2) + f_2(a) \\ \epsilon \dot{d}_2 &= -\delta_R d_2 + \delta_R (y - nd_2)^n (\bar{q}_R - d_2).\end{aligned}\tag{15}$$

By setting $\epsilon = 0$, one obtains the reduced system in the original coordinates, which, since the slow manifold is locally exponentially stable (see the SI), is a good approximation of system (14). This reduced system is given by

$$\begin{aligned}\dot{a} &= -\delta_A a + f_1(a, r) \\ \dot{r} &= \mathcal{S}_R(r, \bar{q}_R)(-\delta_R r + f_2(a))\end{aligned}\tag{16}$$

in which

$$\mathcal{S}_R(r, \bar{q}_R) = \frac{1}{1 + n\bar{q}_R r^{n-1} (1 + r^n)^{-2}}.$$

Since $\mathcal{S}_R(r, \bar{q}_R) \neq 0$, the equilibrium points of (16) are the same as the ones of the isolated system (1). Therefore the unique equilibrium point (a^*, r^*) of (1) is also the unique equilibrium point of (16). We employ the shorthand notation $\mathcal{S}_R^*(\bar{q}_R) := \mathcal{S}_R(r, \bar{q}_R)$. It is easy to verify that $0 < \mathcal{S}_R^*(\bar{q}_R) \leq 1$ and that $\mathcal{S}_R^*(\bar{q}_R)$ is a strictly monotonically decreasing function of \bar{q}_R . Furthermore, we have that

$$\lim_{\bar{q}_R \rightarrow \infty} \mathcal{S}_R^*(\bar{q}_R) = 0 \text{ and } \mathcal{S}_R^*(0) = 1.\tag{17}$$

Hence, the addition of the load to the repressor makes the dynamics of the repressor slower compared to that of the isolated system (1). That is, the repressor *effective* kinetic rates are now smaller by a factor equal to $\mathcal{S}_R^*(\bar{q}_R)$, which can be arbitrarily decreased by increasing the amounts of sites \bar{q}_R . The Jacobian of system (16) calculated at the equilibrium (a^*, r^*) is given by

$$J_R(\bar{q}_R) = \begin{bmatrix} -\delta_A + \frac{\partial f_1(a^*, r^*)}{\partial a} & \frac{\partial f_1(a^*, r^*)}{\partial r} \\ \mathcal{S}_R^*(\bar{q}_R) \frac{\partial f_2(a^*)}{\partial a} & -\mathcal{S}_R^*(\bar{q}_R) \delta_R \end{bmatrix}. \quad (18)$$

Thus, the addition of load to the repressor does not change the sign of the determinant of the Jacobian as $\det(J_R(\bar{q}_R)) = \mathcal{S}_R^*(\bar{q}_R) \det(J_0) > 0$. However, it can change the sign of the trace

$$\text{tr}(J_R(\bar{q}_R)) = -\delta_A + \frac{\partial f_1(a^*, r^*)}{\partial a} - \mathcal{S}_R^*(\bar{q}_R) \delta_R$$

from negative to positive as condition $(ii)'$ is satisfied and condition (17) holds. Hence, the equilibrium point can become unstable with sufficient addition of the load and the system begins oscillating (see the formal derivations in the SI). Figure 4a shows the effect of load on system (14). Note that the parameters were chosen so that the system satisfies conditions (i) and $(ii)'$.

When $\text{tr}(J_R(\bar{q}_R)) = 0$, a Hopf bifurcation occurs since both eigenvalues are imaginary. A continuation analysis can be used to show that this Hopf bifurcation is also present in the full system (14). Figure 4b illustrates that the amount of load required for the Hopf bifurcation is given by $\bar{q}_R = 1.32$ in units of K_{m2} . Hence, the amounts of load needed to switch the clock on is on the same order of the amounts of repressor at the equilibrium. For the LacI repressor employed in [6], $K_{m2} \approx 1pM$ [25], which amounts few copies per cell of the load.

Figure 4c shows that the addition of load increases the period of oscillation. This suggests the possibility that the load can be employed not only for switching an oscillator “on” and “off” but for also tuning the period. However, the increase in period is accompanied by an increase in the amplitude of the oscillation (Figure 4b), which may be undesired. We discuss how the period can be changed while maintaining the amplitude through simultaneous addition of activator and repressor loads in Section “Tuning the Clock period”.

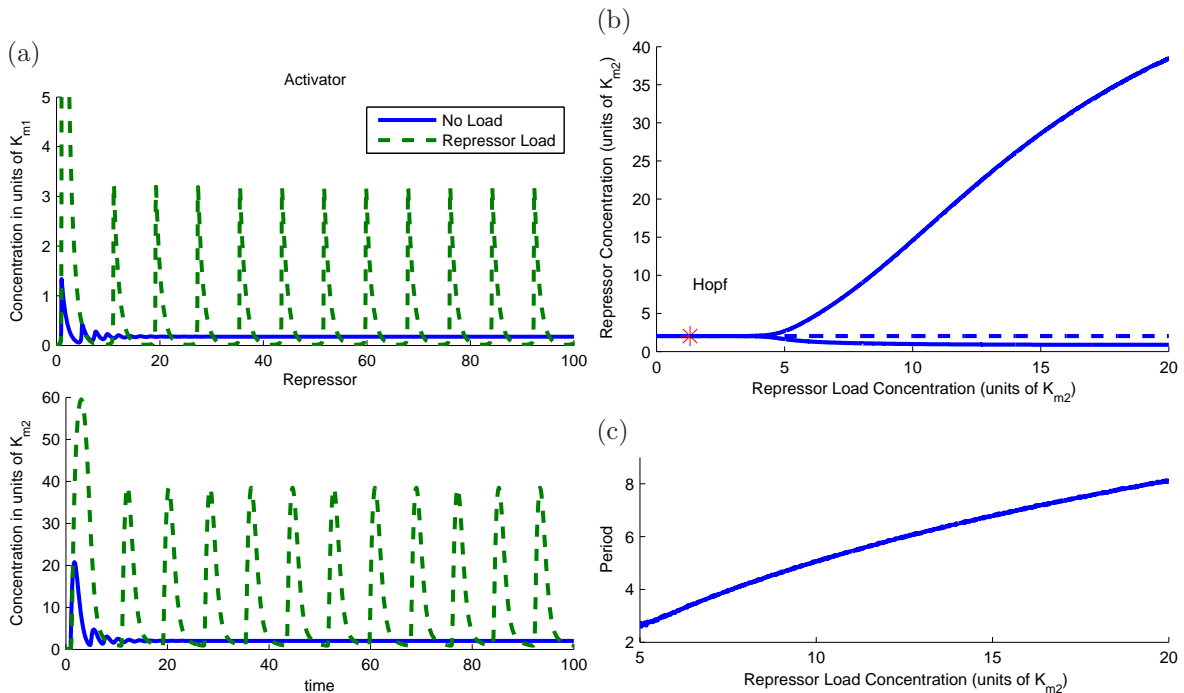


Figure 4. (a) *Load to the Repressor triggers a Non-functional Clock.* The plots illustrate the trajectories of system (14) with two different amounts of load. The parameters in the simulation were $\beta_1 = \beta_3 = 100$, $\beta_2 = .04$, $\beta_4 = .004$, $\delta_A = 1$, $\delta_R = 1.5$, $G_2 = 100$, $m = 2$ and $n = 4$. The amount of DNA binding sites in the system with no load is $\bar{q}_R = 0$ whereas in the system with repressor load is $\bar{q}_R = 20$. (b) *Hopf Bifurcation with \bar{q}_R as a parameter.* A continuation of the equilibrium as a function of the load parameter \bar{q}_R shows that, for this set of parameters, the amount of load required to activate the clock is in the same order of magnitude as that of the affinity coefficient K_{m2} , with bifurcation occurring at $\bar{q}_R = 1.32$. This plot was obtained via continuation of system (14) with the same parameters as before. Solid lines indicate a stable trajectory (limit cycle to the right of the Hopf bifurcation and the equilibrium to its right). The dotted line indicates an unstable equilibrium point. (c) *Period increases as a function of the repressor load \bar{q}_R .*

Stochastic simulations of the switching behavior

In order to understand how robust the switching behavior is to intrinsic noise, we employ stochastic simulations of the system. An implementation of the Gillespie algorithm [26] was employed to produce realizations of trajectories of an activator repressor clock in which both activator and repressor bind to DNA as dimers ($m = n = 2$).

In these simulations, we assumed the presence of 5 copies of each activator and repressor gene to emulate the situation in which the circuit is present in a low copy number plasmid. Expression rates and degradation rates were chosen based on the values used in the deterministic models to obtain a functional and a non-functional oscillator. The association and dissociation rates between proteins and

dimers were chosen so that the apparent dissociation constants $K_{m1} = K_{m2} = 1$, which consider a bacterial transcription factor with apparent dissociation constant on the order of picomolars. A detailed description of this model is given in the SI.

Figure 5a shows that addition of binding sites with affinity to the activator can eliminate oscillations from a functional clock. Figure 5b shows how the addition of binding sites with affinity to the repressor can generate sustained more robust oscillations in a non-functional clock. In both situations, the amount of loads employed to switch the clock is on the order of $10^2 - 10^3$ copies of binding sites per cell, which can be achieved by inserting small arrays in high copy number plasmids.

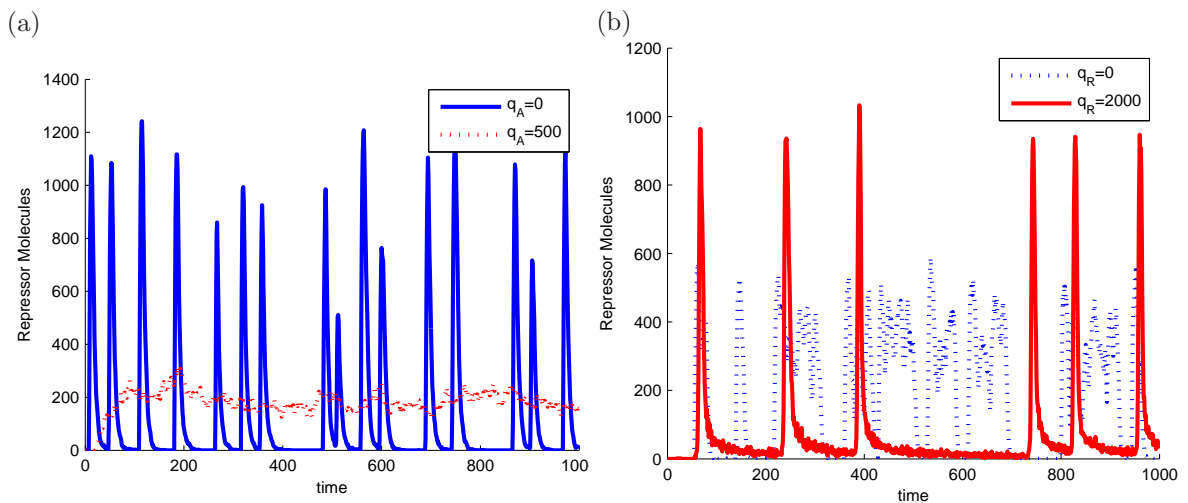


Figure 5. *Effect of the load on clock holds under intrinsic noise.* The plots above are stochastic realizations of an activator-repressor clock with $m = n = 2$ and containing 5 copies of activator and repressor genes. (a) *Functional clock stops with load to the activator.* We show that, with the chosen parameters, it is possible to stop the clock with an amount of load that is roughly 100 times higher than the copy number of the circuit. (b) *Load to the activator leads to robust oscillation.* We show that, the it is possible to generate robust oscillation with roughly 400 times the number of circuit genes with the choice of parameters above.

Tuning the clock period

As noticed in Figure 4c, addition of binding sites to the repressor increases the period of the limit cycles of the system. However, this may cause an increase in the amplitude of the cycle (Figure 4b), which may be undesirable. In this section, we illustrate how the simultaneous addition of load to both the activator and repressor can be employed to vary the period as desired with little impact on the cycle amplitude.

Consider the nondimensional model for the system with DNA binding sites for both the activator and

the repressor as shown in Figure 1d:

$$\begin{aligned}
\dot{A} &= -\delta_A A + g_1(A, R) + k_{u1} D_1 - k_{b1} A^m (q_{A,T} - D_1) \\
\dot{R} &= -\delta_R R + g_2(A) + k_{u2} D_2 - k_{b2} R^n (q_{R,T} - D_2) \\
\dot{D}_1 &= -k'_{u1} D_1 + k'_{b1} A^m (q_{A,T} - D_1) \\
\dot{D}_2 &= -k'_{u2} D_2 + k'_{b2} R^n (q_{R,T} - D_2).
\end{aligned} \tag{19}$$

Here, k_{b1}, k_{u1} model the association and dissociation rates between the activator protein and its corresponding DNA binding site q_A , k_{b2}, k_{u2} model the association and dissociation rates between the repressor protein and its corresponding DNA binding site q_R , $g_1(A, R)$, $g_2(A)$ represent the dimensional version of the Hill functions (see SI), and $q_{A,T}$, $q_{R,T}$ represent the total concentration of activator and repressor DNA sites.

This system can be nondimensionalized, by setting the nondimensional states $a = A/K_{m1}$, $r = R/K_{m2}$, $d_1 = D_1/K_{m1}$ and $d_2 = D_2/K_{m2}$, as shown in the SI, to obtain system

$$\begin{aligned}
\dot{a} &= -\delta_A a + f_1(A, R) + mG_1 \delta_A d_1 - mG_1 \delta_A a^m (\bar{q}_A - d_1) \\
\dot{r} &= -\delta_R r + f_2(A) + nG_2 \delta_R d_2 - nG_2 \delta_R r^n (\bar{q}_R - d_2) \\
\dot{d}_1 &= -G_1 \delta_A d_1 + G_1 \delta_A a^m (\bar{q}_A - d_1) \\
\dot{d}_2 &= -G_2 \delta_R d_2 + G_2 \delta_R r^n (\bar{q}_R - d_2),
\end{aligned} \tag{20}$$

in which $f_1(A, R)$ and $f_2(A)$ are the nondimensional Hill functions as given in expressions (2), $\bar{q}_A = q_{A,T}/K_{m1}$ and $\bar{q}_R = q_{R,T}/K_{m2}$, and G_1 and G_2 are as defined before. In order to employ a singular perturbation argument similar to what was done in the previous sections, define $\epsilon = 1/G_1$, $\nu = G_2/G_1$ to model the explicit timescale separation present in this system. Define also the following change of variables $y_1 := a + md_1$ and $y_2 = r + nd_2$. Substituting these in (20), one obtains the system in standard

singular perturbation form:

$$\begin{aligned}
\dot{y}_1 &= -\delta_A(y_1 - md_1) + f_1(y_1 - md_1, y_2 - nd_2) \\
\dot{y}_2 &= -\delta_R(y_2 - nd_2) + f_2(y_1 - md_1) \\
\epsilon \dot{d}_1 &= -\delta_A d_1 + \delta_A (y_1 - md_1)^m (\bar{q}_A - d_1) \\
\epsilon \dot{d}_2 &= -\nu \delta_R d_2 + \nu \delta_R (y_2 - nd_2)^n (\bar{q}_R - d_2).
\end{aligned} \tag{21}$$

By setting $\epsilon = 0$, one obtains the slow manifold

$$(d_1, d_2) = \left(\bar{q}_A \frac{a^m}{a^m + 1}, \bar{q}_R \frac{r^n}{r^n + 1} \right) := (\phi_1(a), \phi_2(r)).$$

Since the slow manifold is locally exponentially stable (see SI), the reduced system is a good approximation of system (21). Since $\dot{y}_1 = \dot{a} + m \frac{d\phi_1(a)}{da} \dot{a}$ and $\dot{y}_2 = \dot{r} + n \frac{d\phi_2(r)}{dr} \dot{r}$, this reduced system, in the original variables, takes the form

$$\begin{aligned}
\dot{a} &= S_A(a, \bar{q}_A) (-\delta_A a + f_1(a, r)) \\
\dot{r} &= S_R(r, \bar{q}_R) (-\delta_R r + f_2(a)),
\end{aligned} \tag{22}$$

in which

$$S_A(a, \bar{q}_A) = \frac{1}{1 + m \frac{d\phi_1(a)}{da}} = \frac{1}{1 + \bar{q}_A m^2 a^{m-1} (1 + a^m)^{-2}}$$

and

$$S_R(r, \bar{q}_R) := \frac{1}{1 + n \frac{d\phi_2(r)}{dr}} = \frac{1}{1 + \bar{q}_R n^2 r^{n-1} (1 + r^n)^{-2}}.$$

Let the activator and repressor loads be added at a fixed ratio $\rho = \bar{q}_A/\bar{q}_R$ and define $F(a, r, \bar{q}_R) := \frac{S_R(r, \bar{q}_A/\rho)}{S_A(a, \bar{q}_A)}$. System (22) can be re-written as

$$\begin{aligned}
\dot{a} &= (-\delta_A a + f_1(a, r)) S_A(a, \bar{q}_A) \\
\dot{r} &= (-\delta_R r + f_2(a)) S_A(a, \bar{q}_A) F(a, r, \bar{q}_A).
\end{aligned} \tag{23}$$

Since $S_A(a, \bar{q}_A) > 0$, this system is orbitally equivalent [18] to the system

$$\begin{aligned}\dot{a} &= (-\delta_A a + f_1(a, r)) \\ \dot{r} &= (-\delta_R r + f_2(a)) F(a, r, \bar{q}_A).\end{aligned}\tag{24}$$

Hence, if system (23) has a periodic orbit, system (24) will have a corresponding periodic orbit with identical trajectories. The corresponding periodic signals, however, will have different periods whose values depend on function $S_A(a, \bar{q}_A)$. Thus, if the value of $F(a, r, \bar{q}_A)$ does not appreciably change when \bar{q}_A changes, the addition of the load will affect the period of oscillations without impacting their amplitudes. Since

$$\frac{\partial F(a, r, \bar{q}_A)}{\partial \bar{q}_A} = \left(\frac{m^2 a^{m-1}}{(1+a^m)^2} - \rho \frac{n^2 r^{n-1}}{(1+r^n)^2} \right) \frac{(1+r^n)^4}{((1+r^n)^2 + \rho \bar{q}_A n^2 r^{n-1})^2},\tag{25}$$

we have that for large values of \bar{q}_A , $\frac{\partial F(a, r, \bar{q}_A)}{\partial \bar{q}_A} \approx 0$. Under these conditions, since the function $S_A(a, \bar{q}_A)$ is a monotonically decreasing function of \bar{q}_A , the periodic orbits of system (23) will display decreasing periods as \bar{q}_A increases, while maintaining the same amplitude, due to orbital equivalence between system (24) and system (23) (see the SI for a formal proof).

Figure 6a illustrates this result. The addition of repressor load to a functioning clock increases the period but also leads to a higher amplitude. This effect in the amplitude is not observed when both activator and repressor loads are added. Figure 6b shows this behavior for increasing amount of load. When only repressor load is added, there is an increase in the period of the limit cycles along with an increase in the amplitude, as it was seen in the previous section (Figure 4(b) and (c)). However, if a sufficient amount of activator load is simultaneously added along with the repressor load, the increase of the period occurs with very little impact on the amplitude of oscillations.

Discussion

Effective kinetic rates are crucial parameters for the dynamic behavior of biomolecular networks. In particular, delays in negative feedback loops have been shown to be a fundamental mechanism for periodic oscillations both in electronic circuits [27] and in biomolecular networks [1, 10, 15]. Research has shown that in natural systems these delays are realized by the number of steps, such as transcription, translation,

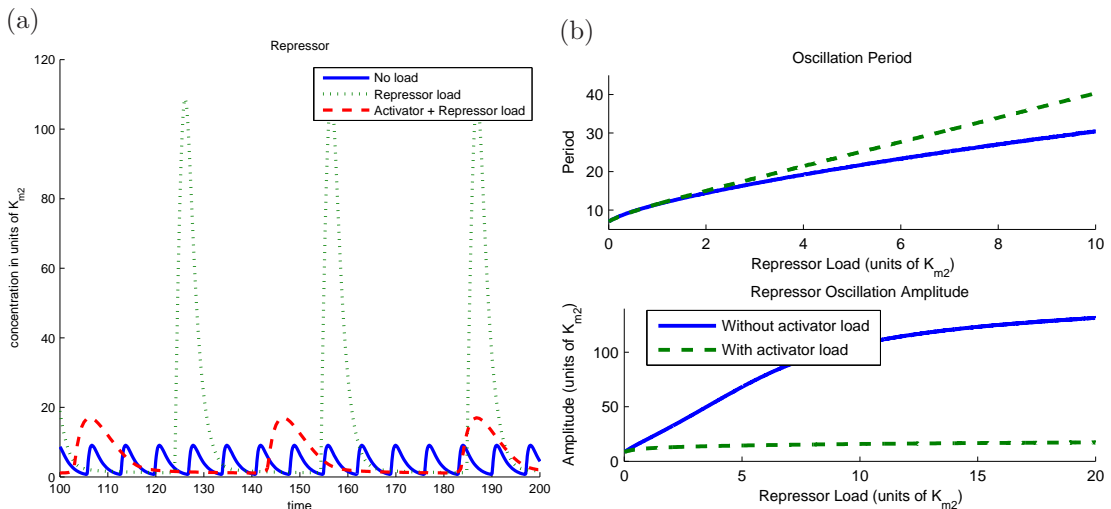


Figure 6. *Tuning the period without affecting the amplitude.* (a) When compared to the isolated system, the amplitude of oscillations in system (20) increases when we add exclusively DNA binding sites with affinity to the repressor ($\bar{q}_A = 0$, $\bar{q}_R = 10$). However, if we simultaneously add DNA binding sites with affinity to the activator, the amplitude is not affected as much ($\bar{q}_A = \bar{q}_R = 10$). (b) The period of system (20) can be changed with no effect on the amplitude when DNA binding sites with affinity to both the repressor and the activator are added simultaneously. The upper plot shows that a similar increase of period observed via the addition of repressor load can be obtained via the simultaneous addition of activator and repressor load. This second method has the advantage of not generating an increase in the amplitude, as shown in the lower plot. In this simulation we assumed the ratio $\rho = \bar{q}_A/\bar{q}_R = 1$. Parameters of the activator repressor system used in the simulation were $\beta_1 = \beta_3 = 100$, $\beta_2 = .04$, $\beta_3 = .004$, $\delta_A = 1$, $\delta_R = 0.5$, $G_1 = G_2 = 100$ and $m = 2$, $n = 4$. In the traces showing only repressor load $\rho = 0$, while the traces showing simultaneous repressor and activator load, $\rho = 1$.

and post-translational modifications, involved in the implementation of the feedback loop. More steps lead to larger delays. Hence, adding a delay involves engineering the structure and length of a pathway. In this paper, we have revealed that a different mechanism exists for adding and carefully tuning delays and effective kinetic rates: the addition of DNA targets. In natural systems, transcription factors can have large numbers of DNA binding sites, several of which do not even have regulatory functions (see [28] and [29], for example). Our study suggests that a role of these DNA binding sites is to carefully tune effective kinetic rates to realize the desired dynamics in genetic networks.

As an example, consider the regulation network of cellular resources such as ribosomes or RNA polymerase (RNAP). Since both molecules need themselves to be assembled, there is a self activating loop. Additionally, it has been shown [30,31] that RNAP and ribosomes are negatively regulated through transcriptional repression. Hence, the regulation motif of these species has the form of Figure 1a, in which we can view A as the resource (RNAP or ribosome) and R as a repressor system. This motif, as

we have shown, can present sustained oscillations, which would be undesired for RNAP or ribosomes. However, due to the large demand by the cellular environment, RNAP and ribosomes are being used through (reversible) binding processes, so that the actual motif is closer to that of Figure 1(b). Since the amount of q is fairly high, the system is brought back to stability.

The capacity of tuning the dynamics stems from the sequestration effect of the protein by the binding sites. The dynamics of the protein slow down because the additional DNA sites increase the demand the system has on the protein. In other words, the protein becomes “busy” having to interact with additional DNA sites. In fact, the technique of employing DNA binding sites to tune a synthetic biomolecular circuit has also been used for reducing the effective concentration of a transcription factor [32]. More generally, this effect can be achieved by employing various protein loads, such as substrates, inhibitors [19], and targets on other proteins [17, 33]. Specifically, the experimental results of [17, 33] show that protein binding domains on other target proteins can function as loads, tuning both protein dynamics and the static characteristics.

The mechanism revealed in this paper for tuning effective kinetic rates is especially relevant for synthetic circuits due to its simple implementation. Instead of modifying promoter or operator regions, or changing degradation tags or protease recognition motifs, a simple addition of DNA with binding sites through transformation or transfection can achieve the desired modifications. This can also simplify prototyping of some synthetic biology modules whose correct function is sensitive to specific kinetic parameters. Gradual addition of DNA sites through inducible plasmids, for example, could be employed to search the parameter space for expected behavior before final adjustment of expression, degradation, and dissociation constants.

Materials and Methods

Simulations were performed using the ode23s numerical solver that comes in MATLAB. Continuation diagrams were made using Matcont. Stochastic simulations were made using an implementation of the Stochastic Simulation Algorithm as described in [26] in a C/POSIX environment. The parameters used in all deterministic simulations are shown in the captions of the figures. Parameters used in the stochastic simulations are given in the Supplementary Information.

Acknowledgments

The authors would like to thank Alessandro Colombo for the useful discussions. This work was in part funded by AFOSR Grant Number FA9550-09-1-0211 and NSF-CIF Grant Number 1058127.

References

1. Novák B, Tyson JJ (2008) Design principles of biochemical oscillators. *Nature reviews Molecular cell biology* 9: 981–91.
2. Alon U (2007) An introduction to systems biology. Design principles of biological circuits. Chapman-Hall.
3. Dunlap JC (1999) Molecular Bases for Circadian Clocks Review. *Cell* 96: 271–290.
4. Ukai H, Ueda HR (2010) Systems biology of mammalian circadian clocks. *Annual review of physiology* 72: 579–603.
5. Vilar JMG, Kueh HY, Barkai N, Leibler S (2002) Mechanisms of noise-resistance in genetic oscillators. *Proceedings of the National Academy of Sciences of the United States of America* 99: 5988–92.
6. Atkinson MR, Savageau MA, Myers JT, Ninfa AJ (2003) Development of Genetic Circuitry Exhibiting Toggle Switch or Oscillatory Behavior in *Escherichia coli*. *Cell* 113: 597–607.
7. Stricker J, Cookson S, Bennett MR, Mather WH, Tsimring LS, et al. (2008) A fast, robust and tunable synthetic gene oscillator. *Nature* 456: 516–9.
8. Danino T, Mondragón-Palomino O, Tsimring LS, Hasty J (2010) A synchronized quorum of genetic clocks. *Nature* 463: 326–30.
9. Tigges M, Marquez-Lago TT, Stelling J, Fussenegger M (2009) A tunable synthetic mammalian oscillator. *Nature* 457: 309–12.
10. Ukai-Tadenuma M, Yamada RG, Xu H, Ripberger Ja, Liu AC, et al. (2011) Delay in feedback repression by cryptochrome 1 is required for circadian clock function. *Cell* 144: 268–81.

11. Relógio A, Westermark PO, Wallach T, Schellenberg K, Kramer A, et al. (2011) Tuning the mammalian circadian clock: robust synergy of two loops. *PLoS computational biology* 7: e1002309.
12. Conrad E, Mayo AE, Ninfa AJ, Forger DB (2008) Rate constants rather than biochemical mechanism determine behaviour of genetic clocks. *Journal of the Royal Society, Interface / the Royal Society* 5 Suppl 1: S9–15.
13. Guantes R, Poyatos JF (2006) Dynamical principles of two-component genetic oscillators. *PLoS computational biology* 2: e30.
14. Del Vecchio D (2007) Design and Analysis of an Activator-Repressor Clock in E. Coli. In: *American Control Conference, 2007. ACC '07. IEEE*, pp. 1589–1594. doi:10.1109/ACC.2007.4282275.
15. Goodwin BC (1963) *Temporal Organization in Cells. A Dynamic Theory of Cellular Control Processes*. New York, NY: Academic Press, 163 pp.
16. Del Vecchio D, Ninfa AJ, Sontag ED (2008) Modular cell biology: retroactivity and insulation. *Molecular Systems Biology* 4: 161.
17. Jiang P, Ventura AC, Merajver SD, Sontag ED, Ninfa AJ, et al. (2011) Load-induced modulation of signal transduction networks. *Science Signaling* 4.
18. Kuznetsov YA (2004) *Elements of Applied Bifurcation Theory*. New York, NY: Springer-Verlag.
19. Barkai N, Leibler S (2000) Circadian clocks limited by noise. *Nature* 403: 267–8.
20. Cantor CR, Schimmel PR (1980) *Biophysical Chemistry: The Behavior of biological macromolecules*. W. H. Freeman, 624 pp.
21. Wiggins S (2003) *Introduction to Applied Nonlinear Dynamical Systems and Chaos*. Springer-Verlag.
22. Khalil HK (2002) *Nonlinear Systems*. Prentice Hall.
23. Kokotović P, Khalil HK, O'Reilly J (1999) *Singular Perturbation Methods in Control*. SIAM.
24. Mutalik VK, Venkatesh KV (2007) A theoretical steady state analysis indicates that induction of *Escherichia coli* glnALG operon can display all-or-none behavior. *Bio Systems* 90: 1–19.

25. Stamatakis M, Mantzaris NV (2009) Comparison of deterministic and stochastic models of the lac operon genetic network. *Biophysical journal* 96: 887–906.
26. Gillespie DT (1977) Exact Stochastic Simulation of Coupled Chemical Reactions. *The Journal of Physical Chemistry* 81: 2340–2361.
27. Schilling DL, Belove C (1968) *Electronic Circuits: Discrete and Integrated*. McGraw Hill.
28. Robison K, McGuire AM, Church GM (1998) A comprehensive library of DNA-binding site matrices for 55 proteins applied to the complete *Escherichia coli* K-12 genome. *Journal of molecular biology* 284: 241–54.
29. Burger A, Walczak AM, Wolynes PG (2010) Abduction and asylum in the lives of transcription factors. *Proceedings of the National Academy of Sciences of the United States of America* 107: 4016–21.
30. Little R, Dennis PP (1979) Expression of RNA polymerase and ribosome component genes in *Escherichia coli* mutants having conditionally defective RNA polymerases. *J of Bacteriology* 137: 115–123.
31. Lemke JJ, Sanchez-Vazquez P, Burgos HL, Hedberg G, Ross W, et al. (2011) Direct regulation of *Escherichia coli* ribosomal protein promoters by the transcription factors ppGpp and DksA. *Proceedings of the National Academy of Sciences of the United States of America* 108: 5712–7.
32. Ozbudak EM, Thattai M, Lim HN, Shraiman BI, Van Oudenaarden A (2004) Multistability in the lactose utilization network of *Escherichia coli*. *Nature* 427: 737–40.
33. Ventura AC, Jiang P, Van Wassenhove L, Del Vecchio D, Merajver SD, et al. (2010) The signaling properties of a covalent modification cycle are altered by a downstream target. *Proc Natl Acad Sci USA* 107: 10032-10037.

1 Supplementary Information

1.1 Model of Hill functions

In this section we identify the Hill function approximations for the expression of proteins controlled by (i) an activator protein and (ii) a repressor and an activator protein. Consider first the expression of protein X whose expression rate is regulated by an activator protein A via the promoter p_R . These processes can be modeled by the following chemical reactions



in which κ_2 is the expression level of the promoter bound to A , κ_4 is the basal expression level of the promoter, k_{a1} and k_{b1} are the association and dissociation rates of the promoter to A respectively and m models the cooperative binding of the activator protein. Assuming that there is a conservation of the total amount of promoter sites, modeled by the expression $p_R + C_1 = p_{R,T}$, the expression level from this promoter can be modeled by $g_2(A) = \kappa_2 C_1(A) + \kappa_4(p_{R,T} - C_1(A))$. The quasi-steady state value of C_1 can be obtained by identifying the equilibrium of the following ODE

$$\dot{C}_1 = k_{a1}(p_{R,T} - C_1)A^m - k_{b1}C_1. \tag{27}$$

Defining $K_{m1} = \sqrt[m]{k_{b1}/k_{a1}}$, we obtain

$$g_2(A) = \kappa_2 p_{R,T} \frac{A^m}{A^m + K_{m1}^m} + \kappa_4 p_{R,T} \frac{K_{m1}^m}{A^m + K_{m1}^m} = \frac{K_2 A^m + K_4 K_{m1}^m}{A^m + K_{m1}^m}, \tag{28}$$

in which $K_2 := \kappa_2 p_{R,T}$ and $K_4 := \kappa_4 p_{R,T}$.

Consider now the expression of a protein X whose expression rate is regulated by an activator protein A as well as by repressor protein R via the promoter p_A . We will assume that the binding is competitive.

Expression can be modeled by the following chemical reactions



in which κ_1 is the expression level of the promoter bound to A , κ_3 is the basal expression level of the promoter, k_{a1} and k_{b1} are the association and dissociation rates of the promoter to A , respectively, k_{a2} and k_{b2} are the association and dissociation rates of the promoter to R , respectively, and m and n model the cooperative binding of the activator and repressor proteins, respectively. We assume that the repressor activity is perfect and therefore no expression can occur from the repressed promoter. Assuming that there is a conservation of the total amount of promoter sites, modeled by the expression $p_A + C_1 + C_2 = p_{A,T}$, the expression level from this promoter can be modeled by $g_1(A, R) = \kappa_1 C_1(A) + \kappa_3(p_{A,T} - C_1(A) - C_2(R))$. The quasi-steady state value of C_1 and C_2 can be obtained by identifying the equilibrium of the following ODE

$$\begin{aligned}
 \dot{C}_1 &= k_{a1}(p_{A,T} - C_1 - C_2)A^m - k_{b1}C_1 \\
 \dot{C}_2 &= k_{a2}(p_{A,T} - C_1 - C_2)R^n - k_{b2}C_2
 \end{aligned} \tag{30}$$

Defining $K_{m1} = (k_{b1}/k_{a1})^{1/m}$ and $K_{m2} = (k_{b2}/k_{a2})^{1/n}$, we obtain the expression

$$g_1(A, R) = p_{A,T} \frac{\kappa_1 K_{m2}^n A^m + \kappa_3 K_{m1}^m K_{m2}^n}{K_{m1}^m K_{m2}^n + K_{m2}^n A^m + K_{m1}^m R^n} = \frac{K_1 K_{m2}^n A^m + K_3 K_{m1}^m K_{m2}^n}{K_{m1}^m K_{m2}^n + K_{m2}^n A^m + K_{m1}^m R^n}, \tag{31}$$

in which $K_1 := \kappa_1 p_{A,T}$ and $K_3 := \kappa_3 p_{A,T}$.

1.2 Nondimensionalization of the activator repressor clock

In this section, we identify a nondimensional model of the activator repressor clock having loads to activator and repressor, given in Figure 1d. The association and dissociation between transcription factor

A and R and their respective additional binding sites q_A and q_R are model by the following dynamics



The model for this system can be obtained by adding the binding dynamics to the model given in [14] for the activator-repressor clock as

$$\begin{aligned} \dot{A} &= -\delta_A A + g_1(A, R) + mk'_{b1} D_1 - mk'_{a1} A^m (q_{A,T} - D_1) \\ \dot{R} &= -\delta_R R + g_2(A) + nk'_{b2} D_2 - nk'_{a2} R^n (q_R - D_2) \\ \dot{D}_1 &= -k'_{b1} D_1 + k'_{a1} A^m (q_{A,T} - D_1) \\ \dot{D}_2 &= -k'_{b2} D_2 + k'_{a2} R^n (q_{R,T} - D_2), \end{aligned} \quad (34)$$

in which $q_{A,T} := q_A + D_1$ and $q_{R,T} := q_R + D_2$ model the total amount of DNA bindings sites in the system, δ_A and δ_R model protein decay (due to either dilution or degradation) and functions f_1 and f_2 model expression rates and take the form of the standard Hill functions derived on Section 1.1.

$$g_1(A, R) = \frac{K_1(A/K_{m1})^m + K_3}{1 + (A/K_{m1})^m + (R/K_{m2})^n} \text{ and } g_2(A) = \frac{K_2(A/K_{m1})^m + K_4}{1 + (A/K_{m1})^m}, \quad (35)$$

in which K_1 and K_2 are the maximal expression rates, K_3 and K_4 represent the basal expression, K_{m1} and K_{m2} is related to the affinity between the proteins and their respective binding sites and m and n are the Hill coefficients related to the multimerization of activator and repressor proteins, respectively. Define $G_1 := k'_{b1}/\delta_A$ and $G_2 := k'_{b2}/\delta_R$ to be non-dimensional constants modeling the timescale difference between complex dissociation and transcription factor degradations rates. Define additionally $K'_{m1} := \sqrt[n]{k'_{b1}/k'_{a1}}$ and $K'_{m2} = \sqrt[m]{k'_{b2}/k'_{a2}}$ as the apparent dissociation constant as defined in [20].

From this system, define the nondimensional variables $a := A/K_{m1}$, $r := R/K_{m2}$, $d = D_1/K'_{m1}$ and $d_2 = D_2/K'_{m2}$. Let $\sigma_1 = K'_{m1}/K_{m1}$ and let $\sigma_2 = K'_{m2}/K_{m2}$ describe the difference in affinity of the transcription factor to the promoter in the circuit or the additional DNA load. The differential equation

is then reduced to

$$\begin{aligned}
\dot{a} &= -\delta_A a + \frac{\beta_1 a^m + \beta_2}{1 + a^m + r^n} + mG_1 \delta_A \sigma_1 d_1 - mG_1 \delta_A \sigma_1^{(1-m)} a^m (\bar{q}_A - d_1) \\
\dot{r} &= -\delta_R r + \frac{\beta_3 a^m + \beta_4}{1 + a^m} + nG_2 \delta_R \sigma_2 d_2 - nG_2 \delta_R \sigma_2^{(1-n)} r^n (\bar{q}_R - d_2) \\
\dot{d}_1 &= -G_1 \delta_A d_1 + G_1 \delta_A \sigma_1^{-m} a^m (\bar{q}_A - d_1) \\
\dot{d}_2 &= -G_2 \delta_R d_2 + G_2 \delta_R \sigma_2^{-n} r^n (\bar{q}_R - d_2),
\end{aligned} \tag{36}$$

in which $\beta_1 := K_1/K_{m1}$, $\beta_2 := K_A/K_{m1}$, $\beta_3 := K_2/K_{m2}$, $\beta_4 := K_R/K_{m2}$, $\bar{q}_A = q_{A,T}/K'_{m1}$ and $\bar{q}_R = q_{R,T}/K'_{m2}$.

From system (36), one can obtain non-dimensional models for the various systems described in this paper. In particular, to obtain (1), $\bar{q}_R = \bar{q}_A = 0$; in (5) $\bar{q}_R = 0$ and $\sigma_1 = 1$; in (14) $\bar{q}_A = 0$ and $\sigma_2 = 1$ and finally in (20) $\sigma_1 = \sigma_2 = 1$.

1.3 Conditions for a unique and unstable equilibrium

We next establish parameter conditions for which we can guarantee that there is a unique equilibrium of system (1).

Let $\bar{\beta}_1 = \beta_1/\delta_A$, $\bar{\beta}_2 = \beta_2/\delta_A$, $\bar{\beta}_3 = \beta_3/\delta_R$, $\bar{\beta}_4 = \beta_4/\delta_R$ and let

$$f(a, r) := -\delta_A a + f_1(a, r) \text{ and } g(a, r) := -\delta_R r + f_2(a, r). \tag{37}$$

Then, the nullclines are given by $f(a, r) = 0$ and $g(a, r) = 0$, which define r as a function of a in the following way:

$$f(a, r) = 0 \implies r = \left(\frac{\bar{\beta}_1 a^m + \bar{\beta}_2 - a(1 + a^m)}{a} \right)^{1/n} \tag{38}$$

$$g(a, r) = 0 \implies r = \frac{\bar{\beta}_3 a^m + \bar{\beta}_4}{1 + a^m}. \tag{39}$$

Proposition 2. *If $m = 1$, system (1) admits a unique stable equilibrium point. If $m = 2$, system (1) admits a unique unstable (not locally a saddle) equilibrium point if the following parameter relations are verified*

$$0 < \bar{\beta}_2 \leq \frac{\bar{\beta}_1^3}{27}, \quad L \leq \frac{\bar{\beta}_3 A_L^2 + \bar{\beta}_4}{1 + A_L^2}, \quad l \geq \frac{\bar{\beta}_3 A_l^2 + \bar{\beta}_4}{1 + A_l^2}, \tag{40}$$

and

$$\left. \frac{\delta_R}{\partial f_1 / \partial a} \right|_{(a^*, r^*)} - \delta_A < 1, \quad (41)$$

in which

$$\begin{aligned} A_l &= \frac{\bar{\beta}_1}{6} \left(1 - (\cos(\phi/3) - \sqrt{3}\sin(\phi/3)) \right) \\ A_L &= \frac{\bar{\beta}_1}{6} + \frac{\bar{\beta}_1}{3} \cos(\phi/3) \\ \phi &= \operatorname{atan} \left(\frac{\sqrt{27\bar{\beta}_2(\bar{\beta}_1^3 - 27\bar{\beta}_2)}}{\frac{\bar{\beta}_1^3}{2} - 27\bar{\beta}_2} \right), \end{aligned} \quad (42)$$

$$l = \sqrt[n]{\frac{\bar{\beta}_1 A_l^2 + \bar{\beta}_2 - A_l(1 + A_l^2)}{A_l}},$$

$$L = \sqrt[n]{\frac{\bar{\beta}_1 A_L^2 + \bar{\beta}_2 - A_L(1 + A_L^2)}{A_L}}.$$

Proof. The Jacobian at $S^* := (a^*, r^*)$ is given by the matrix

$$J(S^*) = \begin{pmatrix} \frac{\partial f}{\partial a} & \frac{\partial f}{\partial r} \\ \frac{\partial g}{\partial a} & \frac{\partial g}{\partial r} \end{pmatrix},$$

in which the partial derivatives are computed at the equilibrium point S^* . For an unstable node or spiral to occur, it is sufficient that

$$(i) \operatorname{tr}(J(S^*)) > 0 \text{ and } (ii) \det(J(S^*)) > 0.$$

Case 1: $m = 1$. The nullcline $f(a, r) = 0$ has always negative slope, and therefore we always have only one equilibrium point. Furthermore, expression (38) with $m = 1$ leads to

$$\left. \frac{dr}{da} \right|_{f(a,r)=0} = -\frac{r^{-1+1/n} a^2 + \bar{\beta}_2}{n a^2} < 0.$$

Since $dr/da|_{f(a,r)=0} = -(\partial f / \partial a) / (\partial f / \partial r)$ by the implicit function theorem and since $\partial f / \partial r < 0$, it must be that $\partial f / \partial a < 0$. As a consequence, $\operatorname{tr}(J(S^*)) < 0$ because $\frac{\partial g}{\partial r} = -\delta_R < 0$. To show that both eigenvalues of $J(S^*)$ are negative, we are left to show that $\det(J(S^*)) > 0$. This is readily seen to be

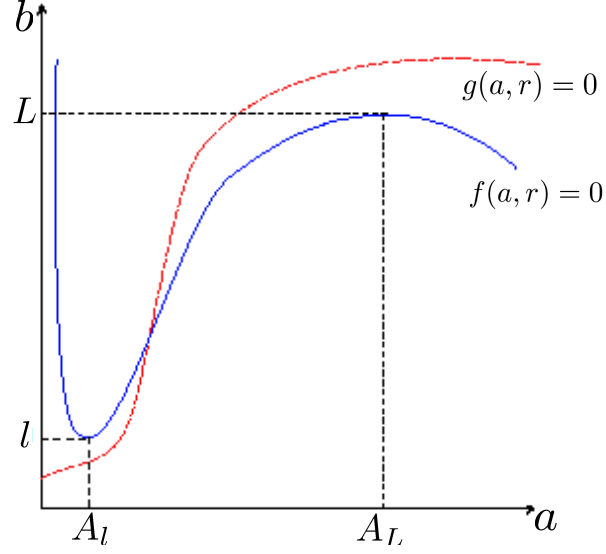


Figure 7. Nullclines and the values A_L , A_l , L , and l .

true as we have that

$$\left. \frac{dr}{da} \right|_{g(a,r)=0} = -\frac{\partial g/\partial a}{\partial g/\partial r} > \left. \frac{dr}{da} \right|_{f(a,r)=0} = -\frac{\partial f/\partial a}{\partial f/\partial r} < 0,$$

thus implying that $\frac{\partial f}{\partial a} \frac{\partial g}{\partial r} - \frac{\partial f}{\partial r} \frac{\partial g}{\partial a} = \det(J(S^*)) > 0$.

Case 2: $m = 2$. Figure 7 shows the only possible configuration of the nullclines in which (a) we have a unique equilibrium and (b) the nullclines are intersecting with the same positive slope. The plots imply that

$$\left. \frac{dr}{da} \right|_{g(a,r)=0} = -\frac{\partial g/\partial a}{\partial g/\partial r} > \left. \frac{dr}{da} \right|_{f(a,r)=0} = -\frac{\partial f/\partial a}{\partial f/\partial r} > 0,$$

and thus that $\frac{\partial f}{\partial a} \frac{\partial g}{\partial r} - \frac{\partial f}{\partial r} \frac{\partial g}{\partial a} = \det(J(S^*)) > 0$. By relations (37), we have that $\partial g/\partial a = \partial f_2/\partial a$, $\partial g/\partial r = -\delta_R$, $\partial f/\partial a = (-\delta_A + \partial f_1/\partial a)$, and $\partial f/\partial r = -|\partial f_1/\partial r|$. If at the equilibrium point S^* the nullcline $f(a, r) = 0$ has negative slope, S^* is stable, as we have shown for the case $m = 1$. Therefore, we examine what additional conditions should be enforced to guarantee that the equilibrium point is unstable when the nullclines intersect both with positive slopes. Since condition (ii) is verified by the condition that the nullclines cross with positive slopes, we are left to provide conditions for which (i) is also true. To have that $\text{tr}(J(S^*)) > 0$, we require that $(\frac{\partial f_1}{\partial a} - \delta_A) - \delta_R > 0$, which is verified if condition (41) holds.

We finally determine sufficient conditions on the parameters for having one crossing and such that the

slopes of the two nullclines at the crossing are both positive (and thus (ii) is verified). This is performed by simple geometric considerations. For this purpose, consider Figure 7.

The values A_I and A_L of the location of the minimum and maximum of $f(a, r) = 0$ can be computed by computing the derivative with respect to A of expression

$$r^n = \frac{\bar{\beta}_1 a^2 + \bar{\beta}_2 - a(1 + a^2)}{a}$$

obtained by (38) and equating it to zero, as the square root function is monotone. This way, we find a third order polynomial that has two positive roots if $0 < \bar{\beta}_2 \leq \frac{\bar{\beta}_1^3}{27}$, otherwise it has one positive and two complex roots. These roots are given by relations (42) and they are shown in Figure 7. Thus, by looking at the same figure, one deduces that if conditions (40) are satisfied, we have on equilibrium point only, and (ii) is verified. \square

For having one equilibrium point only, we require the activator basal transcription rate, proportional to $\bar{\beta}_2$, to be sufficiently smaller than the maximal expression rate of the activator, which is proportional to $\bar{\beta}_1$. Also, $\bar{\beta}_2$ must be non-zero. Also, in case $\bar{\beta}_1 \gg \bar{\beta}_2$, one can verify that $A_L \approx \bar{\beta}_1/2$ and thus $L \approx \sqrt[3]{\bar{\beta}_1^2/4}$. As a consequence, conditions (40) require also that if $\bar{\beta}_1$ increases then so must do $\bar{\beta}_3$. This qualitatively implies that the maximal expression rate of the repressor must be larger than the maximal expression rate of the activator, when expressed in units of the affinity constant. Finally, $A_I \approx 0$ and $l \approx \sqrt[3]{\bar{\beta}_2/A_I}$. As a consequence, conditions (40) also imply that the smaller $\bar{\beta}_2$ becomes, the smaller $\bar{\beta}_3$ must be.

1.4 Proofs on the effect of load

Proposition 3. *Consider system (10) satisfying conditions (i) and (ii). There exists $q^* > 0$ such that the equilibrium (a^*, r^*) is asymptotically stable if and only if $\bar{q}_A > q^*$.*

Proof. We first show that $\det(J_A(\bar{q}_A)) > 0$ for all \bar{q}_A . This follows from the fact that $\det(J_A(\bar{q}_A)) = \mathcal{S}_A^*(\bar{q}_A) \det(J_0) > 0$, from condition (i). We now focus on

$$\text{tr}(J_A(\bar{q}_A)) = \mathcal{S}_A^*(\bar{q}_A) \left[-\delta_a + \frac{\partial f_1(a^*, r^*)}{\partial a} \right] - \delta_R.$$

From (11) and condition (ii), when $\bar{q}_A = 0$ $\text{tr}(J_A(0)) > 0$. Additionally, as $\bar{q}_A \rightarrow \infty$, $\text{tr}(J_A(\bar{q}_A)) \rightarrow$

$-\delta_R < 0$. Since the trace is a monotonic smooth function of \bar{q}_A , one can apply the intermediate value theorem to show that there is a unique $0 < q^* < \infty$ such that $\text{tr}(J_A(q^*)) = 0$. Since $\det(J_A(q^*)) > 0$, the eigenvalues of $J_A(q^*)$ are imaginary. From the monotonicity of the trace with respect to \bar{q}_A , it follows that the real parts of the eigenvalues of $J_A(\bar{q}_A)$ are positive for all $0 \leq \bar{q}_A < q^*$ and negative for all $\bar{q}_A > q^*$. It follows that the system goes through a Hopf bifurcation at $\bar{q}_A = q^*$, and thus presents a periodic solution for $0 \leq q_A < q^*$ while it converges to the equilibrium for $\bar{q}_A > q^*$. \square

Proposition 4. *Consider system (16) satisfying conditions (i) and (ii)'. There exists a $q^* > 0$ such that the equilibrium (a^*, r^*) is asymptotically stable if and only if $\bar{q}_R < q^*$.*

Proof. We first show that the $\det(J_R(\bar{q}_R)) > 0$ for all q_R . This follows from the fact that $\det(J_R(\bar{q}_R)) = \mathcal{S}_R^*(\bar{q}_R) \det(J_0) > 0$ from condition (i). We now proceed to show that the trace can change its sign. Note that

$$\text{tr}(J_R(\bar{q}_R)) = -\delta_A + \frac{\partial f_1(a^*, r^*)}{\partial a} - \mathcal{S}_R^*(\bar{q}_R) \delta_R.$$

From (17) and condition (ii)', when $\bar{q}_R = 0$, $\text{tr}(J_R(\bar{q}_R)) < 0$. Additionally, as $\lim_{\bar{q}_R \rightarrow \infty} \text{tr}(J_R(\bar{q}_R)) = -\delta_A + \frac{\partial f_1(a^*, r^*)}{\partial a} < 0$ from condition (ii)'. Since the trace is a monotonic smooth function of \bar{q}_R , one can apply the intermediate value theorem to show that there is a unique $0 < q^* < \infty$ such that $\text{tr} J_R(q^*) = 0$. Since $\det(J_R(q^*)) > 0$, the eigenvalues of $J_R(q^*)$ are imaginary. From the monotonicity of the trace with respect to \bar{q}_R , it follows that the real parts of the eigenvalues of $J_R(\bar{q}_R)$ are negative for all $0 \leq \bar{q}_R < q^*$ and positive for all $q_R > q^*$. It follows thus that the system goes through a Hopf bifurcation at $\bar{q}_R = q^*$ and thus presents a periodic solution for $\bar{q}_R > q^*$ while it converges to the equilibrium for $\bar{q}_R < q^*$. \square

1.5 Proofs on stability of the slow manifolds

Proposition 5. *The stability of the slow manifold $d_1 = \psi_1(y)$ defined by setting $\epsilon = 0$ in system (7-9) is locally exponentially stable.*

Proof. The manifold $d_1 = \psi_1(y)$ is the unique solution of the algebraic equation

$$g(y, d_1) := -\delta_A d_1 + \delta_A (y - m d_1)^m (q_T - d_1) = 0.$$

Note that, since $0 \leq d_1 \leq q_T$, $0 \leq \psi_1(y) \leq q_T$.

To prove this proposition, we need to show that $\left. \frac{\partial g(y, d_1)}{\partial d_1} \right|_{d_1=\psi_1(y)} < 0$ [22].

$$\frac{\partial g(y, d_1)}{\partial d_1} = -\delta_A - m\delta_A(y - md_1)^{m-1}(\bar{q}_A - d_1) - \delta_A(y - md_1)^m.$$

Since $g(y, \psi_1(y)) = 0$, $y - m\psi_1(y) = \sqrt[n]{\frac{\psi_1(y)}{\bar{q}_A - \psi_1(y)}}$ and therefore

$$\left. \frac{\partial g(y, d_1)}{\partial d_1} \right|_{d_1=\psi_1(y)} = -\delta_A - m\delta_A \left(\frac{\psi_1(y)}{\bar{q}_A - \psi_1(y)} \right)^{\frac{m-1}{m}} (\bar{q}_A - \psi_1(y)) - \delta_A \frac{\psi_1(y)}{\bar{q}_A - \psi_1(y)} < 0,$$

since $0 \leq \psi_1(y) \leq \bar{q}_A$ for all values of y as shown above. \square

Proposition 6. *The stability of the manifold $d_2 = \psi_2(y)$ defined by setting $\epsilon = 0$ in system (15) is locally exponentially stable.*

Proof. The proof of this result is similar to the proof of the previous proposition. Here we must show that $\left. \frac{\partial h(y, d_2)}{\partial d_2} \right|_{d_2=\psi_2(y)} < 0$ where the manifold $d_2 = \psi_2(y)$ is the unique solution of equation

$$h(y, d_2) := -\delta_R d_2 + \delta_R (y - nd_2)^n (\bar{q}_R - d_2) = 0.$$

Since $0 \leq d_2 \leq \bar{q}_R$, $0 \leq \psi_2(y) \leq \bar{q}_R$. Additionally, from the definition of the manifold, $y - n\psi_2(y) = \sqrt[n]{\frac{\psi_2(y)}{q + R - \psi_2(y)}}$. Therefore

$$\begin{aligned} \left. \frac{\partial h(y, d_2)}{\partial d_2} \right|_{d_2=\psi_2(y)} &= -\delta_R - n\delta_R (y - n\psi_2(y))^{n-1} (\bar{q}_R - \psi_2(y)) - \delta_R (y - n\psi_2(y))^n \\ &= -\delta_R - n\delta_R \left(\frac{\psi_2(y)}{\bar{q}_R - \psi_2(y)} \right)^{\frac{n-1}{n}} (\bar{q}_R - \psi_2(y)) - \delta_R \frac{\psi_2(y)}{\bar{q}_R - \psi_2(y)} < 0. \end{aligned}$$

\square

Proposition 7. *The stability of the manifold $(d_1, d_2) = (\psi_1(y_1), \psi_2(y_2))$ defined by setting $\epsilon = 0$ in system (21) is locally exponentially stable.*

Proof. Define $g(y_1, d_1) := -\delta_A d_1 + \delta_A (y_1 - md_1)^m (\bar{q}_A - d_1) = 0$ and $h(y_2, d_2) := -\delta_R d_2 + \delta_R (y_2 - nd_2)^n (\bar{q}_R - d_2) = 0$. The manifold $(d_1, d_2) = (\psi_1(y_1), \psi_2(y_2))$ is defined such that $g(y_1, \psi_1(y_1)) = 0$ and

$h(y_2, \psi_2(y_2)) = 0$. To prove the local exponential stability of the manifold, we need to show that the Jacobian

$$J = \begin{bmatrix} \frac{\partial g(y_1, d_1)}{\partial d_1} & \frac{\partial g(y_1, d_1)}{\partial d_2} \\ \frac{\partial h(y_2, d_2)}{\partial d_1} & \frac{\partial h(y_2, d_2)}{\partial d_2} \end{bmatrix} = \begin{bmatrix} \frac{\partial g(y_1, d_1)}{\partial d_1} & 0 \\ 0 & \frac{\partial h(y_2, d_2)}{\partial d_2} \end{bmatrix}.$$

calculated at the manifold $(d_1, d_2) = (\psi_1(y_1), \psi_2(y_2))$ has negative eigenvalues. Since this is a diagonal matrix, the problem is reduced to proving that the two following inequalities hold:

$$\begin{aligned} \left. \frac{\partial g(y_1, d_1)}{\partial d_1} \right|_{d_1=\psi_1(y_1)} &< 0 \\ \left. \frac{\partial h(y_2, d_2)}{\partial d_2} \right|_{d_2=\psi_2(y_2)} &< 0. \end{aligned} \quad (43)$$

From the definition of the manifold,

$$0 \leq \psi_1(y_1) \leq \bar{q}_A \text{ and } 0 \leq \psi_2(y_2) \leq \bar{q}_R.$$

Additionally,

$$y_1 - \psi_1(y_1) = \sqrt[m]{\frac{\psi_1(y_1)}{\bar{q}_A - \psi_1(y_1)}} \text{ and } y_2 - \psi_2(y_2) = \sqrt[n]{\frac{\psi_2(y_2)}{\bar{q}_R - \psi_2(y_2)}}.$$

Therefore

$$\begin{aligned} \left. \frac{\partial g(y_1, d_1)}{\partial d_1} \right|_{d_1=\psi_1(y_1)} &= -\delta_A - \delta_A \left(\frac{\psi_1(y_1)}{\bar{q}_A - \psi_1(y_1)} \right)^{\frac{m-1}{m}} (\bar{q}_A - \psi_1(y_1)) - \delta_A \frac{\psi_1(y_1)}{\bar{q}_A - \psi_1(y_1)} < 0 \\ \left. \frac{\partial h(y_2, d_2)}{\partial d_2} \right|_{d_2=\psi_2(y_2)} &= -\delta_R - \delta_R \left(\frac{\psi_2(y_2)}{\bar{q}_R - \psi_2(y_2)} \right)^{\frac{n-1}{n}} (\bar{q}_R - \psi_2(y_2)) - \delta_R \frac{\psi_2(y_2)}{\bar{q}_R - \psi_2(y_2)} < 0. \end{aligned} \quad (44)$$

□

1.6 Proofs on orbital equivalence

Proposition 8. *Consider the following ordinary differential equations*

$$\dot{x} = f(x) \tag{45}$$

$$\dot{x} = g(x) = \mu(x)f(x), \tag{46}$$

in which $x \in \mathbb{R}^n$, $f : \mathbb{R}^n \rightarrow \mathbb{R}^n$ is Lipschitz continuous and $0 < a \leq \mu(x) \leq b < \infty$ is a Lipschitz continuous scalar function. Then, there exists a function $\alpha : \mathbb{R} \rightarrow \mathbb{R}$, monotonically increasing and bounded such that if $\phi(t)$, $t \in \mathbb{R}^n$ is a solution of (45) with initial condition $x = x_0$, then $\psi(t) := \phi(\alpha(t))$, is a solution of (46) with the same initial conditions. Furthermore, $\frac{d\alpha(t)}{dt} = \mu(\phi(\alpha(t)))$.

Proof. Since $\phi(t)$ is a solution of (45), for all $t > 0$, we have that $\frac{d\phi(t)}{dt} = f(\phi(t))$. Let $\alpha(t)$ be the solution of the ordinary differential equation

$$\frac{d\alpha}{dt} = \mu(\phi(\alpha)) \tag{47}$$

with initial condition $\alpha(0) = 0$. Let also $\psi(t)$ be defined as above. Since $g(x)$ is Lipschitz continuous, system (46) has an unique local solution at the point $\psi(t)$ whose tangent is given by $g(\psi(t))$. The vector tangent to $\psi(t)$ is given by

$$\frac{d\psi(t)}{dt} = \frac{d\phi(\alpha(t))}{dt} = \frac{d\phi(\alpha)}{d\alpha} \frac{d\alpha(t)}{dt} = f(\psi(t))\mu(\psi(t)) = g(\psi(t)) \tag{48}$$

for all t . Additionally, note that $\alpha(0) = 0$ and therefore $\psi(0) = \phi(0) = x_0$. It follows that $\psi(t)$ is the solution for (46) with initial condition $x = x_0$. \square

The following proposition is used to show that the addition of load will increase the period.

Proposition 9. *Consider the ordinary differential equations (45-46) under the same conditions as in Proposition 8. Assume that (45) has a periodic solution $\phi(t)$ with period T . If $\mu(x) < 1$, then the solution of (46) is a periodic solution with period $T' > T$.*

Proof. From Proposition 8, we have that $\psi(t) := \phi(\alpha(t))$ is a solution for (46), in which $\alpha(t)$ satisfies the

differential equation

$$\frac{d\alpha(t)}{dt} = \mu(\phi(\alpha(t))). \quad (49)$$

Since the solution $\alpha(t)$ is monotonic and unbounded and since $\alpha(0) = 0$, for all $T > 0$, there is $T' > 0$ such that $\alpha(T) = T'$. Since $\phi(T) = \phi(0)$, $\psi(T') = \psi(0)$, and hence ψ is periodic with period T' . From (49) and the fact that $\mu(x) < 1$,

$$T' = \alpha(T) = \int_0^T \mu(\phi(\alpha(t))) dt < \int_0^T 1 dt = T. \quad (50)$$

□

1.7 Mechanistic Model for Stochastic Simulation

For the analysis employing the stochastic simulation algorithm [26], we considered a mechanistic model that includes all the reactions in Table 1. Table 2 gives the description the states.

This system is equivalent to the system 20 with $m = n = 2$. We consider a one-step model for protein expression and assume the rate of expression is a function of whether the promoter p_A and p_R are free, bound to an activator dimer and bound to a repressor dimer in the case of p_A . Additionally, we consider the dynamics of the dimerization of both transcription factors.

The degradation rate δ_R was the parameter chosen to generate a model for a functioning and a non-functioning clock. The total number of promoters in both simulations was $p_{A,T} = p_{R,T} = 5$. Changes in the number of binding sites q_A and q_R were used to generate retroactivity to the activator and repressor respectively.

Table 1. Reactions considered in the mechanistic model

Reaction	Description	Rate	Value
$2R \rightarrow R_2$	Repressor Dimerization	k_{ra}	200
$R_2 \rightarrow 2R$	Repressor Monomerization	k_{rb}	200
$2A \rightarrow A_2$	Activator Dimerization	k_{aa}	200
$A_2 \rightarrow 2A$	Activator Monomerization	k_{ab}	200
$p_R + A_2 \rightarrow C_3$	Activator Binding	k_{a1}	2000
$C_3 \rightarrow p_R + A_2$	Activator Dissociation	k_{b1}	2000
$C_3 \rightarrow C_3 + R$	Repressor Maximal Expression	κ_3	100
$p_R \rightarrow p_R + R$	Repressor Basal Expression	κ_4	.004
$p_A + A_2 \rightarrow C_1$	Activator Binding	k_{a1}	2000
$C_1 \rightarrow p_A + A_2$	Activator Dissociation	k_{b1}	2000
$p_A + R_2 \rightarrow C_2$	Repressor Binding	k_{a2}	2000
$C_2 \rightarrow p_A + R_2$	Repressor Dissociation	k_{b2}	2000
$C_1 \rightarrow C_1 + A$	Activator Maximal Expression	κ_1	100
$p_A \rightarrow p_A + A$	Activator Basal Expression	κ_2	.04
$A \rightarrow \emptyset$	Activator Monomer Degradation	δ_A	1
$R \rightarrow \emptyset$	Repressor Monomer Degradation	δ_R	.2 / .4
$A_2 \rightarrow \emptyset$	Activator Dimer Degradation	δ_A	1
$R_2 \rightarrow \emptyset$	Repressor Dimer Degradation	δ_R	.2 / .4
$q_A + A_2 \rightarrow D_1$	Activator-Load Binding	k_{a1}	2000
$D_1 \rightarrow q_A + A_2$	Activator-Load Dissociation	k_{b1}	2000
$q_R + R_2 \rightarrow D_2$	Repressor-Load Binding	k_{a1}	2000
$D_2 \rightarrow q_R + R_2$	Repressor-Load Dissociation	k_{b1}	2000

Table 2. Species in mechanistic model

State	Species
R	Repressor Monomer
R_2	Repressor Dimer
A	Activator Monomer
A_2	Activator Dimer
p_R	Promoter Regulating Repressor Expression
p_A	Promoter Regulating Activator Expression
C_1	Promoter-Activator Complex, Activator Expression
C_2	Promoter-Repressor Complex, Activator Expression
C_3	Promoter-Activator Complex, Repressor Expression
q_A	Load with affinity to the activator
q_R	Load with affinity to the repressor
D_1	Activator-Load Complex
D_2	Repressor-Load Complex